The CP43 Proximal Antenna Complex of Higher Plant Photosystem II Revisited: Modeling and Hole Burning Study. I

Nhan C. Dang,[†] Valter Zazubovich,[‡] Mike Reppert,[†] Bhanu Neupane,[†] Rafael Picorel,[§,⊥] Michael Seibert,[§] and Ryszard Jankowiak*,[†]

Department of Chemistry, Kansas State University, Manhattan, Kansas 66506, Department of Physics, Concordia University, Montreal H4B1R6, Quebec, Canada, and National Renewable Energy Laboratory, Golden, Colorado 80401

The CP43 core antenna complex of photosystem II is known to possess two quasi-degenerate "red"-trap states (Jankowiak, R. et al. *J. Phys. Chem. B* **2000**, *104*, 11805). It has been suggested recently (Zazubovich, V.; Jankowiak, R. *J. Lumin.* **2007**, *127*, 245) that the site distribution functions of the red states (A and B) are uncorrelated and that narrow holes are burned in the subpopulations of chlorophylls (Chls) from states A and B that are the lowest-energy Chl in their complex and previously thought not to transfer energy. This model of uncorrelated excitation energy transfer (EET) between the quasidegenerate bands is expanded by taking into account both electron–phonon and vibrational coupling. The model is applied to fit simultaneously absorption, emission, zero-phonon action, and transient hole burned (HB) spectra obtained for the CP43 complex with minimized contribution from aggregation. It is demonstrated that the above listed spectra can be well-fitted using the uncorrelated EET model, providing strong evidence for the existence of efficient energy transfer between the two lowest energy states, A and B (either from A to B or from B to A), in CP43. Possible candidate Chls for the low-energy A and B states are discussed, providing a link between CP43 structure and spectroscopy. Finally, we propose that persistent holes originate from regular NPHB accompanied by the redistribution of oscillator strength due to excitonic interactions, rather than photoconversion involving Chl–protein hydrogen bonding, as suggested before (Hughes J. L. et al. *Biochemistry* **2006**, *45*, 12345). In the accompanying paper (Reppert, M.; Zazubovich, V.; Dang, N. C.; Seibert, M.; Jankowiak, R. *J. Phys. Chem. B* **2008**, 9934), it is demonstrated that the model discussed in this manuscript is consistent with excitonic calculations, which also provide very good fits to both transient and persistent HB spectra obtained under non-line-narrowing conditions.

1. Introduction

The photosystem II (PSII) core contains two antenna proteins, CP43 and CP47, and the D1/D2/cytochrome (Cyt) b_{559} reaction center (RC), where charge separation occurs.[1,2] The two core antenna complexes are present in all oxygenic photosynthetic organisms in a constant ratio of 1:1 with respect to the D1/D2/Cyt b_{559} RC complex. The assembly of these three pigment–protein complexes along with the extrinsic 17-, 23-, and 33-kDa proteins compose the O_2-evolving PSII core complex.[1,3] CP43 seems to be more loosely bound to the D1/D2 heterodimer than CP47, since it is easier to remove from the PSII core complex. The CP43 complex is responsible for light-harvesting and energy transfer to the RC and may be involved in stabilization of the oxygen-evolving complex,[4,5] whereas CP47 in addition to its light-harvesting and energy-transfer functions is believed to play a role in the dimerization of the PSII core.[4–6] The crystal structure of PSII (first determined at 3.8-Å resolution in 2001;[7] available online under protein databank (PDB) ID number 1FE1) was recently refined to 3.0-Å (PDB ID number 2AXT), where it was shown that CP43 contains 13 chlorophyll *a* (Chl *a*)

molecules;[8] that is, one Chl less than previously suggested[9] (PDB ID number 1S5L). The structure of the monomeric PSII RC and CP43 complex (view from the stromal side), taken from Loll et al.[8] is shown in Figure 1. The structure on the right represents the reaction center; the Chls on the left correspond to the CP43 complex.

The main function ascribed to CP43 is as a proximal antenna that funnels excitation energy from LHCII (the major antenna complex of PSII) and CP29, CP26, and CP24 (minor PSII antenna complexes) to the reaction center.[10] It is also involved in maintaining the structure of the PSII complex and sustaining the assembly of this supramolecular complex within the thylakoid membrane.[6,10,11] The CP43 complex is also very sensitive to conditions under which PSII is photoinhibited. This may correlate with the close proximity of CP43 to the D1 RC polypeptide, known to be the main target of the photoinhibition process.[12–14]

The CP43 complex consists of a single polypeptide (the *psbC* gene product) of 43-kDa apparent molecular mass.[15] It was first isolated by lithium dodecyl sulfate electrophoresis[16,17] and recently by liquid chromatography.[18–21] Dependent on the purification procedure used, most absorption spectra[18,21] have shown the presence of a main band near 669–671 nm and a minor one at 682–683 nm. The relative ratio of these two bands is sample-dependent (vide infra). This could indicate that some denaturing occurs during purification or that samples contain
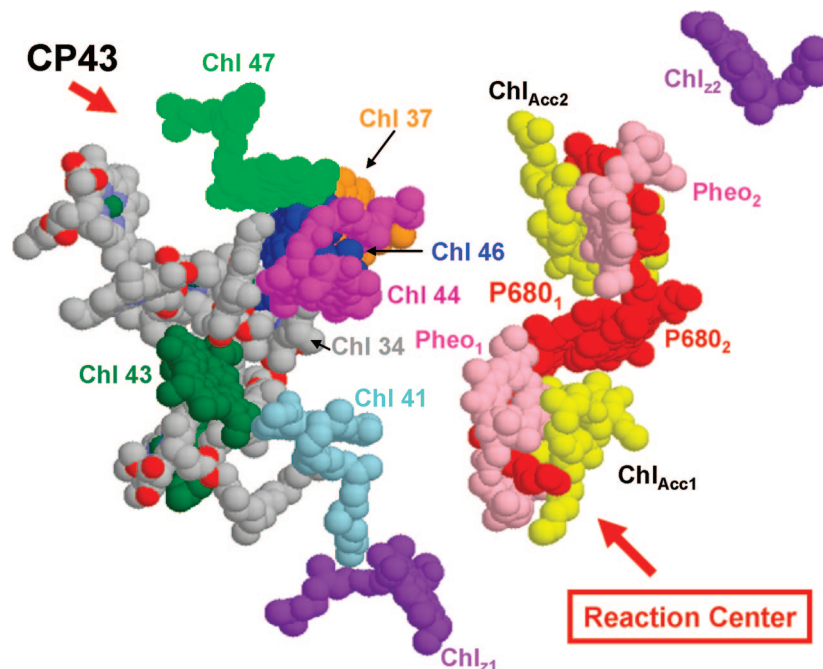
* Corresponding author. E-mail: ryszard@ksu.edu.
† Kansas State University.
‡ Concordia University.
§ National Renewable Energy Laboratory.
⊥ Permanent address: Estacion Experimental Aula Dei (CSIC), Apdo. 202, 5580 Zaragoza, Spain.

Figure 1. Structure of CP43 and the photosystem II reaction center.

different amounts of CP43 aggregates.[18] Although typical fluorescence spectra have shown a major emission band near 684−684 nm, indicating efficient energy transfer among all pigments in the CP43 complex, additional fluorescence contributions near 675, 680, and 685−686 nm were also present,[18,21] depending on the sample quality.

It has been known for awhile that CP43 possesses two quasi-degenerate, lowest-energy states (A and B in the notation of Jankowiak et al.[22]), one of which, namely, state B, is characterized by an unusually narrow inhomogeneous bandwidth. Gaussian fitting of the absorption spectrum indicated that the red absorption region can be fitted only if there is an additional broadband,[21] thus suggesting the presence of two different sets of red-absorbing pigments. This two-state model is consistent with fluorescence line-narrowing experiments, which showed[21] that emission (upon excitation below 685 nm) from two different pools of Chls was observed. The presence of two different pools of Chl was also confirmed by HB experiments;[22–24] however, the precise origin of the bands A and B is unclear. Early excitonic calculations,[25] in which it was assumed that transition dipoles of all Chl molecules are oriented in the membrane plane, suggested that broader-band A might be due to an ensemble of strongly coupled chlorophylls, but these preliminary calculations (based on the 3.8-Å structure of Zouni et al.[7]), were unable to reproduce the narrow band B near 683 nm.[42] It should be emphasized that these early excitonic calculations[25] were intended as only a preliminary modeling attempt and are unreliable as the new higher-resolution CP43 structure reveals that the transition dipoles of several Chl are significantly out of the membrane plane; additionally, the 3.8 Å structure used in previous calculations did not contain Chl 47 (in the notation of Loll et al.[8]). It has been suggested that state B owes its peak position and narrow bandwidth to the unusual protein environment of the respective chlorophyll.[18,22] Since in this model we have a single Chl contributing to the B state and several Chls contributing to the A state, we will refer to this model as B1AM, where M stands for multiple pigments. Very recently, evidence has been presented, which is based on the results of time-domain, room-temperature (RT) experiments, that the chloro-

phyll responsible for the B band is weakly coupled to the rest of the pigments in the CP43.[23] This paper also contains some discussion on possible assignments of the B state.

On the other hand, the CD spectra[24] indicate that narrow band B has significant rotational strength, which appears to be inconsistent with the assignment of the B state to a monomeric chlorophyll. Hughes et al.[24] suggested that band B is the lowest excitonic state of a relatively strongly coupled chlorophyll ensemble, with two other states of the same ensemble peaked at ∼680 and 676.5 nm. This conclusion was based on the analysis of the changes in the CD spectra upon nonresonant higher-energy illumination at 4 K. They also suggested that band A is due to a state well-localized on a single Chl *a*. We will refer to this proposal as the BMA1 model (vide infra).

Straightforward comparison of these two models (i.e., B1AM and BMA1) is difficult because experimental data were obtained for samples with different ratios of absorption at 683 and 685 nm. Different ratios render more or less support for B1AM or BMA1 models; however, one cannot exclude that the real origin of the differences in that ratio is just a different (sample-dependent) contribution from aggregated or denatured CP43 complexes. (Detergent concentration-dependent contribution from aggregates was already suggested in ref 18). In other words, a possible contribution from "nonnative" samples in the spectral range of 685−688 nm complicates a straightforward assignment (vide infra) of states B and A.

It is also unclear how far apart the Chls responsible for the A and B bands are located within the CP43 complex and if they are connected by energy transfer. Originally, we suggested, on the the basis of the ability to burn dephasing-limited holes anywhere within the wavelength range corresponding to the A and B bands,[18] that excitation energy transfer (EET) between those two states is very slow, and respective pigments could be situated on the opposite sides of the complex. However, we have recently demonstrated that the CP43′ complex of PSI isolated from cyanobacteria grown under iron-starvation stress conditions, which is homologous to the CP43 complex of PSII, also possesses A and B states and that the results can be explained better if one allows for EET between these two states

CP43 Antenna Complex of Higher Plant Photosystem

J. Phys. Chem. B, Vol. 112, No. 32, 2008 **9923**

on a $\sim$10-ps time scale.[26] As a result, in a brief communication, we have proposed a model, involving EET between quasi-degenerate states with uncorrelated site distribution functions (SDFs), that qualitatively explains the hole-burning data for both CP43 and CP43′.

In this manuscript, we simultaneously fit absorption and emission spectra, the zero-phonon action spectrum, and the main band of the transient HB spectrum (for samples with minimized contribution from aggregates) to demonstrate that EET between the pigments with uncorrelated SDFs has to be considered when interpreting optical spectra obtained for the CP43 complex. Our improved model takes into account both electron−phonon and vibrational coupling. Finally, we discuss the compatibility of our data with the B1AM and BMA1 models mentioned above, as well as with B1A1 (vide infra). The impact of aggregation on absorption and hole-burned spectra will also be discussed.

2. Materials and Methods

2.1. Preparation of CP43 Antenna Complex. The CP43 isolation procedure was a modification of that reported by Alfonso et al.[19] and Groot et al.[21] as described in Jankowiak et al.[18] In the present work, an additional chromatography column was used at the end of the earlier purification procedure. The material eluted from the Q-Sepharose column with $10-70$ mM $MgSO_4$ linear gradient in 50 mM Tris−HCl, pH 7.8, plus 0.03% (w/v) n-dodecyl β-D-maltoside (DM) was dialyzed against 20 mM Bis-Tris, pH 6.0, plus 0.03% (w/v) DM and passed through a DEAE TSK Toyoepearl 650s column equilibrated with the same dialysis buffer. The material that did not bind to the column was collected and constituted the CP43 complex used in this work. The CP43 complex exhibited a room temperature absorption spectrum with a peak at 669.8 nm and a pronounced shoulder at 683 nm. Part of the sample material was mixed with an equal volume of a glycerol/ethylene glycol (55/45, v/v) mixture to a final optical density of about 0.6 at the maximum peak in the red, and the rest was concentrated with 30-kDa cutoff Amicon Centricon tubes up to an optical density (OD) of about 25. Samples were kept at -80 °C until used. All preparation procedures were carried out in dim light at 4 °C. The samples were diluted for low temperature absorption, fluorescence, and hole-burning spectroscopy experiments (see figure captions for details) with a glycerol/ethylene glycol (55/45, v/v) mixture to ensure good glass formation. To minimize or eliminate contribution from aggregation and photodamage to the CP43 complexes, sample handling was done at 10 °C in the presence of very dim light. To minimize aggregation, sonication in the dark at 10 °C was performed shortly before each experiment. Samples diluted shortly before the experiment (from high-OD samples (OD = 25)) routinely provided absorption spectra with decreased contribution from aggregated CP43 and a higher intensity band near 683 nm in comparison with the major band near 670 nm.

2.2. Spectroscopic Measurements. The hole-burning setup used is described elsewhere.[27] Briefly, absorption and HB spectra were recorded with a Bruker HR125 Fourier transform spectrometer at a resolution of 4 or 0.5 cm^{-1}, respectively. Nonresonant burning was performed with the green light optimized at 496.5 nm from a Coherent Innova 200 Ar$^+$ ion laser. A tunable Coherent CR699-21 ring dye laser (line width of 0.07 cm^{-1}, laser dye; DCM Special (Exciton)), pumped by a 6-W Coherent Innova 90 Ar$^+$ ion laser, was used for resonant hole-burning. The intensity of the CR699-21 laser beam was stabilized electrooptically (Brockton Electro-Optics Corp., LPC) and was attenuated using a set of neutral density filters. The persistent nonphotochemical hole-burned spectra reported cor-

respond to the postburn absorption spectrum minus the preburn absorption spectrum. The triplet bottleneck (transient) hole-burned spectra correspond to absorption spectrum with laser *on* minus the spectrum with laser *off*. Transient hole spectra were measured after the persistent hole-burning process had reached saturation. Burn wavelengths, intensities, and times are given in the figure captions. The sample temperature was maintained at 4.2 K using a Janis 8-DT Super Vari-Temp liquid helium cryostat. The temperature was stabilized and measured with a Lakeshore Cryotronic model 330 temperature controller. Low-temperature fluorescence spectra were obtained with excitation wavelength of 496.5 nm from the Coherent Innova 200 Ar$^+$ ion laser. Fluorescence was dispersed by a 300-mm-focal-length monochromator and detected by a PI Acton Spec-10 (1340 × 400) CCD camera. The full width at half-maximum (fwhm) of spectral resolution for fluorescence spectra was $\sim$0.1 nm. For fluorescence measurements, the OD of the samples was reduced to 0.1/1 cm sample thickness (at the absorption maximum), and the sample thickness was reduced to $\sim$1 mm to ensure that reabsorption effects were negligible. When bringing the spectra measured with FTIR spectrometer and with spectrograph/CCD to the same frequency or wavelength scale, it was taken into account that the refraction index of air is 1.0003.

2.3. Capillary Electrophoresis (CE) Interfaced with Low-Temperature Fluorescence Detection. CE has been interfaced with low-temperature fluorescence spectroscopy for online detection and high-resolution spectroscopic identification of various separated analytes.[28,29] In this methodology the use of low temperatures alleviates the problems of possible photodegradation, whereas online detection allows the sequential characterization and identification of the separated (i.e., compositionally "pure") analyte zones in the capillary.[30,31] The system consists of a modular CE apparatus, the instrumentation for low temperature fluorescence detection, and a specially designed capillary cryostat (CC); for details see refs 28, 29. Briefly, the CC consists of a double-walled quartz cell with an inlet line for introducing liquid helium. The outer portion of the CC is evacuated. The capillary, positioned in the central region of the CC, is quickly cooled to 4.2 K by a continuous flow of liquid helium. The CC is attached to a precision translation stage. Translation of the CC and capillary in the direction of the capillary axis allows the separated analytes to be sequentially characterized by low temperature spectroscopy as the capillary is translated through the laser excitation region. In this work, we have used this instrumentation to reseparate a typical preparation of the CP43 complex. Separation conditions werethe following: 20 mM Bis−Tris, 20 mM NaCl, 0.1% (w/v) DM, 10% (w/v) glycerol; 25 kV ($\sim$20 mA), capillary 75 μm (i.d.). Low temperature ($T = 4.2$ K) fluorescence spectra obtained online for the major separated peaks were obtained with $\lambda_{ex} = 351.1$ nm and are discussed below.

3. Results

3.1. Low-Remperature Absorption and Emission Spectra of CP43 Complexes. Q$_y$-region 4.2 K absorption and fluorescence spectra of three different samples of the CP43 core antenna protein complex are shown in Figure 2, frames A and B, respectively. All three samples were obtained from the same preparation, but they were handled differently before spectroscopic measurements were taken. Sample 1 was stored in a glycerol/ethylene glycol matrix in the freezer (-77 °C) for several weeks before use. Samples 2 and 3 were stored in buffer at high OD before dilution (with glycerol/ethylene glycol) to OD $\sim$ 0.6 immediately before use in experiment. In addition,
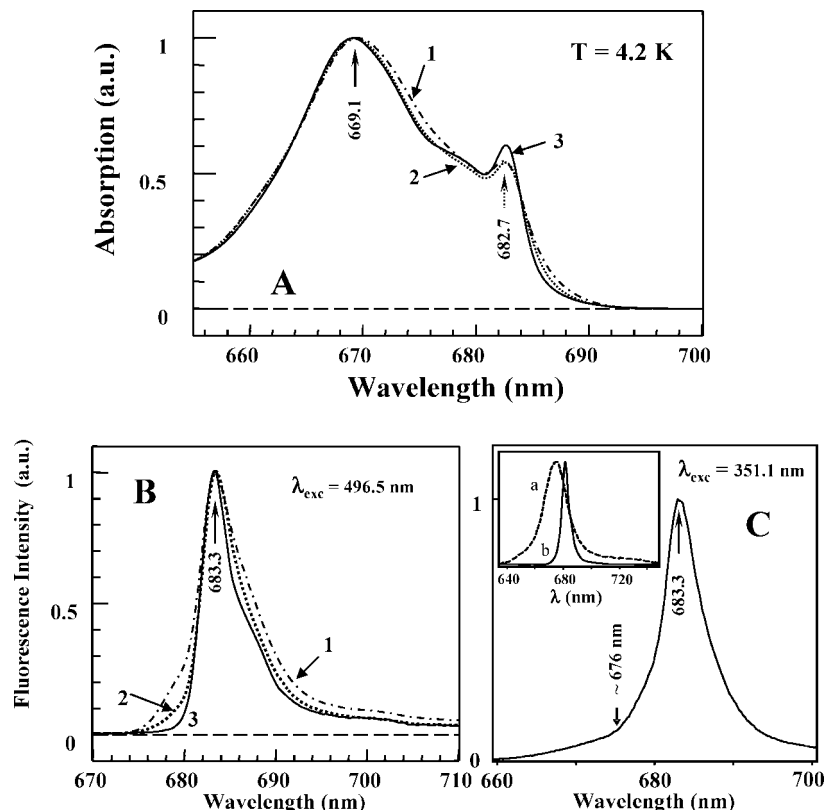
Figure 2. Absorption (frame A) and emission spectra (frame B) obtained for three different CP43 samples (solid curve for the sample 3, dotted for sample 2, and dotted−dashed for sample 1). Frame C shows the fluorescence spectrum ($\lambda_{ex} = 351.1$ nm) of an old CP43 sample with significant contribution near 676 nm. The insert of Frame C shows that this contribution (curve *a*) can be separated from the main fluorescence spectrum (curve *b*) by capillary electrophoresis (see text for details). All fluorescence spectra were obtained at $T = 4.2$ K.

after dilution, sample 3 was sonicated in the dark in a cold water bath before use. In general, both absorption and emission spectra are similar to the CP43 spectra published previously.[18,21,24] That is, all absorption spectra show two major maxima near 683 and 670 nm and a shoulder at ~678 nm. However, a close inspection reveals several important differences: spectrum 3 (in particular) has a narrower Q_y absorption profile than spectra 1 and 2 with a maximum at 669.1 nm, stronger shoulder near 678 nm, and somewhat weaker absorption near 675 nm. Most importantly, spectrum 3 has more intense narrow absorption at 682.7 nm and weaker absorption near the 685−687-nm region, likely associated in part with a contribution from aggregated CP43[18] (vide infra). On the basis of many spectra obtained for the CP43 complex in our laboratory during the past decade, as well as the literature data on CP43,[21,24] we suggest that the more intact the CP43 preparation, the more intense the band near 683 nm should be observed. The 4th derivative (not shown for brevity) of the absorption spectrum 3 clearly indicated that absorption near 683 nm region contains contribution from at least two absorption bands, in agreement with previous results.[18,23,24] More experimental data that support this view will be presented below. For convenience of description, the bands contributing to the 683 nm absorption band, as before,[18,22] are labeled below as A (broad one) and B (narrow one).

The fluorescence spectra shown in Figure 2B (i.e., curves 1−3) correspond to the absorption spectra labeled 1, 2, and 3 in Frame A and were obtained at 4.2 K with an excitation wavelength of 496.5 nm. All spectra have a fluorescence maximum near 683.3 nm. The spectral position of absorption and emission spectra suggests a very small Stokes shift, in agreement with previous data;[18] however, the shape and width of all three spectra is very different. (The spectra are normalized

at the peak near 683 nm.) In particular, spectrum 3, in contrast to spectra 1 and 2, does not possess any emission band near 679 nm and reveals less emission in the 685−687 nm region; note that aggregated CP43 complexes have an emission maximum in the 685−687 nm region.[18] Repeated experiments on many different CP43 preparations showed that these complexes are very sensitive to photodamage and denaturing, showing (depending on sample) a variable contribution of the 679 nm emission band, as well as emission from aggregated CP43 complexes with the (0, 0)-emission band near 685−687 nm. Interestingly, the more photodamaged a preparation is, the more emission near 679 nm is observed, suggesting the presence of partly damaged complexes.

It should be noted that none of the three samples (curves 1−3 in Figure 2B) show emission in the 665−677 nm range which is associated with fluorescence of disconnected Chls or contamination by other minor complexes (e.g., CP29; vide infra), as previously observed in several published CP43 fluorescence spectra.[18,19] For comparison, a fluorescence spectrum obtained from an earlier preparation (similar to the emission spectra published previously[18]) is shown in frame C of Figure 2, where, as before, additional broad fluorescence in the 665−677 nm region is clearly observed. To show that this contribution does not belong to the CP43 complex and most likely is not due to a contribution from disconnected Chls (whose emission maximum is expected near 670−673 nm,[21] we used our capillary electrophoresis (CE) system interfaced with low-temperature laser-induced fluorescence (LIF) spectroscopy.[28,29] The findings are summarized in the insert of Figure 2C. The CP43 sample with the emission spectrum shown in frame 2C was separated into two components by CE (Figure 2C insert) with fluorescence maxima at 676 nm (curve a) and 683.3 nm (curve b),
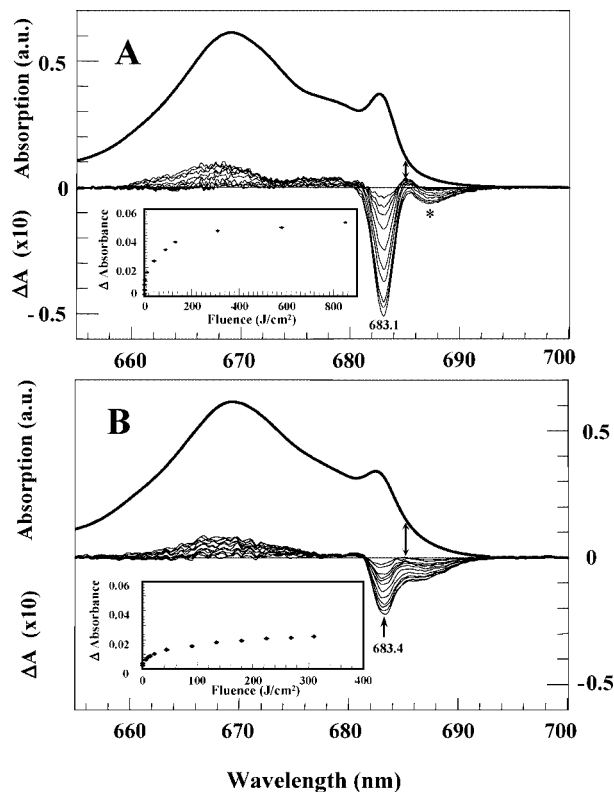
Figure 3. Comparison of hole burning in two samples with different degrees of aggregation. Frame A shows fluence dependence of spectral holes burned at 496.5 nm for a sample with a lesser degree of aggregation. The asterisk indicates contribution from the A band. Frame B shows hole-burning in a sample with a greater degree of aggregation. The hole-burning conditions are similar to that of frame A. The two-sided arrow indicates absorption maximum of aggregated CP43 complexes. The inset in frames A and B shows the development of hole depth as a function of fluence; see text for details.

respectively (fluorescence of the separated components was detected online by LIF). Thus, the broad emission near 676 nm (indicated by a solid arrow) could be separated from the intact CP43 complex whose integrated intensity accounted for about 85% of total emission. Thus, we conclude the minor component in the "old" CP43 preparation corresponds to a small contamination, most likely by the CP29 complex whose (0, 0)-emission band is known to lie near 676 nm.[18] Thus, it appears that most (if not all) published emission spectra of CP43 complexes[18,19,21] could have been contaminated by the above-discussed contribution. On the other hand, aggregation is difficult to control, and its contribution (variable from sample to sample) is difficult to eliminate. That is, even our "best" CP43 preparation (spectrum 3, Figure 2B), as demonstrated below, contains a small contribution from aggregated CP43 complexes (see Section 4.4).

3.2. Persistent and Transient Hole Burned Spectra. Frames A and B in Figure 3 show quite similar absorption spectra but very different HB spectra obtained for two different CP43 samples (samples 3 and 2, respectively, from Figure 2A). The absorption spectrum shown in frame B is very similar to the published absorption spectra in refs 18 and 24 and has a much weaker absorption band near 683 nm and more intensity in the 687-nm region (see double arrow), which is associated with aggregates of CP43 complexes. As a result, the main hole is red-shifted by about 0.3 nm, and no clear antihole near 685 nm (originating mostly from the B state; vide infra) is observed in frame B. This is due to the lower peak intensity at ~683 nm. Since the peak at 683 nm is lower in the absorption shown
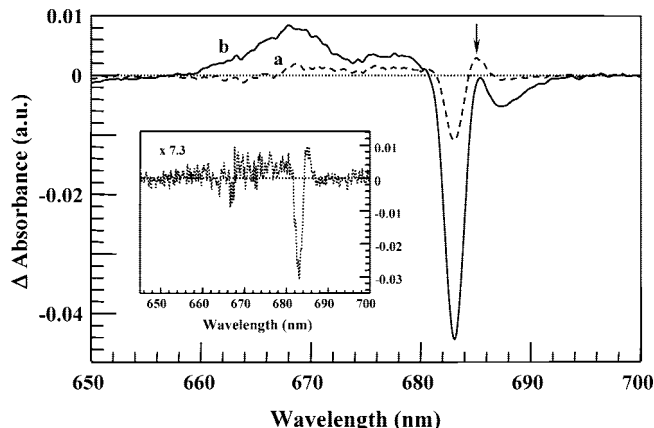

Figure 4. Hole-burning phenomena in CP43 during interaction with green light (496.5 nm). Inset shows a hole spectrum in a very early hole burning stage (fluence = 1.25 J/cm²) whereas spectra a and b were burnt with fluence of 4.7 and 311.3 J/cm², respectively. Note, solid arrow shows photoproduct forming on the lower energy side of the hole (see text for more details).

in frame B, most likely there is less B state available for HB. Assuming that B burns more efficiently than A, this would also explain why the burning efficiency is lower in this particular sample.

Frame A shows the CP43 absorption spectrum with the most intense 683 nm band (sample 3) observed so far and quite different HB spectra when compared with data shown in frame B. In this case, at least at the early stage of hole burning, the 685-nm antihole is more clearly observed due to a minimized hole burning into the origin band of aggregates (i.e., less aggregated sample). In addition, samples with a relatively larger contribution from aggregated CP43 complexes (see frame B) show significantly decreased hole depth at 683 nm (by a factor of ~2 at about 300 J/cm²) obtained for the same fluence, as illustrated in the inserts of frames A and B of Figure 3. This behavior, at least in part, is likely due to the fact that a more intact CP43 sample (whose spectra are shown in frame A of Figure 3) has more contribution from the A and B bands (in particular, the B band) than any previously published absorption spectrum.[18,21,22,24] This is consistent with a much narrower emission spectrum originating from both the A and B bands (see Figure 2B), as further discussed below. These data clearly demonstrate that the shape and depth of persistent HB spectra strongly depend on sample quality.

In agreement with earlier studies,[18] at low irradiation doses, the hole spectrum, peaking at ~683 nm, is dominated by band B and provides information on the photoproduct distribution of band B. Interestingly, the narrow antihole due to the nonphotochemical hole burning (NPHB) can be observed mostly at lower energy with respect to the hole. One cannot rule out some contribution to this band from photoproduct due to burning of the low-energy fraction of band A or to aggregates, but this contribution is negligibly small at low fluences. This is depicted more clearly in Figure 4 where curves a and b were obtained nonresonantly for two different fluences, 4.7 and 311.3 J/cm,² respectively. To demonstrate that the hole feature near 688 nm develops only at higher fluences, an additional HB spectrum that was obtained with a fluence of 1.25 J/cm² is shown in the inset of Figure 4. All HB spectra shown in Figures 3 and 4 were obtained at 4.2 K using a burning wavelength of 496.5 nm. The maximum of the major nonresonant hole shown in the insert of Figure 4 ($\Delta OD \sim 0.05$; i.e., 13% hole) is located at 683.1 nm (14 639 cm⁻¹), in good agreement with the intense
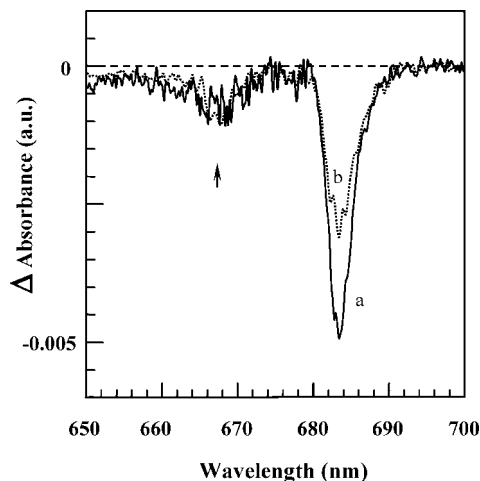
Figure 5. Transient (triplet-bottleneck) spectral holes burned at 496.5 nm for samples with a low (solid curve a, sample 3) and high (dotted curve b; sample 1) degree of aggregation. Corresponding absorption spectra for samples 1 and 3 are shown in Figure 2 (frame A).

~683-nm absorption band shown as curve 3 in Figure 2. A Gaussian fit of the 683.1-nm hole (obtained for the fluence of 1.25 J/cm^2) yielded a width of 33 cm^{-1}, slightly narrower than in our earlier reported data (i.e., 45 cm^{-1}).[18] As before, we refer to this hole as the B state. However, the hole shown in the insert of Figure 4 reaches a width of 45 cm^{-1} at saturation conditions, in perfect agreement with our earlier data.[18] That is, at higher irradiation doses, the holes become broader due to contribution from band A.

However, it is obvious (in particular, for saturated holes) that the delta-absorbance increase is distributed at various wavelengths well beyond the inhomogeneous widths of bands A and B, most notably in the region to the blue of 670 nm. It has been recently suggested[24] that a novel process referred to as photoconversion, as opposed to regular NPHB, could account for this behavior. Although this positive absorbance increase could originate from a photoconversion process that involves Chl−protein hydrogen bonding, as suggested recently in ref 24, it also could be caused by a redistribution of oscillator strength due to modified site excitation energies and excitonic interactions during the burning process. This latter interpretation is in good agreement with the appearance of an excitonically coupled hole in the same spectral region (i.e., 660−675 nm) in triplet bottleneck hole-burning spectra shown in Figure 5 (vide infra). Interestingly, a hole previously observed[18] at ~680 nm and correlated with a feature near 683 nm in the CD spectrum is hardly discernible in our HB spectra shown in Figures 3 and 4. Theoretical fits (based on excitonic calculations) of the shape of the persistent holes shown in Figure 4, which take into account the contribution from antiholes (originating from the NPHB processes into the A and B bands) are beyond the scope of this paper, but they are presented in the accompanying paper and are in good agreement with the data presented in this manuscript.

Below, we will focus on a fit of a nonresonantly burned transient hole which, by the nature of the transient hole-burning process, is free from photoproduct contribution. An example of the 4.2 K triplet-bottleneck-hole spectra of CP43 obtained with burning wavelength of 496.5 nm for sample 3 (solid line; curve a) and sample 1 (dotted line; curve b) are shown in Figure 5. As before,[18] a broad hole near 683 nm is clearly observed. In contrast to the results shown in ref 18, where burning wavelengths of 665 or 670 nm were used, the illumination was

at 496.5 nm, and as a result, no resonant transient features are present within the Q$_y$ absorption band. The hole in curve a (our best sample 3) is highly asymmetric and has a fwhm of ~82 cm^{-1} (once again narrower than the 120 cm^{-1} reported earlier,[18] clearly indicating relatively more contribution from the B band in comparison with sample 1 (curve b) and our earlier transient spectra obtained for CP43 samples.[18] Spectra a and b cannot be easily normalized because they clearly have different contributions from the B band (see Figure 3) and from band A. As a result, the hole near 683 nm in spectrum a has more contribution from sub-band B$_s$ (see Sections 4.1–4.3 for details) and slightly different shape of the band near 669 nm. Since the two spectra shown in Figure 5 are very similar in the low-energy region, it appears that aggregates do not contribute significantly to the transient spectra.

The transient hole peaked at ~683 nm was previously assigned to the A band alone.[18] However, current results support the conclusion of ref 22 that both bands (A and B) contribute to the 683-nm transient hole, in agreement with the sample-dependent width of the triplet-bottleneck hole. The difference between our current interpretation and ref 18 is that in our current model, only the subensembles A$_s$ or B$_s$ of A and B pigments, which are the lowest energy pigment in their complex (and therefore incapable of further downhill energy transfer) contribute to transient hole burned spectra. The same is true for the saturated (nonresonantly burned) persistent holes shown in Figures 3 and 4. The holes near 683 and 669 nm seem to be correlated, since a bleaching at ~669 nm was also observed for burning near 675 nm (data not shown); see also ref 18. Thus, we believe that the transient satellite hole near 669 nm in Figure 5 (see solid arrow) originates from burning in the A and B bands and is most likely due to the chlorophylls excitonically coupled to pigments A or B or both (see the accompanying paper). Thus, it is not surprising that the shape of the 669-nm hole is different for samples with relatively different contribution from the A$_s$ or B$_s$ substates (vide infra). Again, no features at 680 nm could be observed in our transient holes in agreement with our previous results.[18]

A transient HB spectrum (which, as mentioned above, does not reveal any NPHB antiholes or photoproducts) can be used to test various models; namely, we will show below that to properly fit absorption and transient HB spectra simultaneously with the zero-phonon action spectrum and fluorescence spectra, one has to take into account the energy transfer between quasidegenerate A and B states that have uncorrelated SDFs as originally suggested in refs 18 and 22 (see Sections 4.1–4.4.

3.3. Zero-Phonon Action Spectra. ZPH-action spectroscopy is another mode for investigating the lowest energy states of the CP43 antenna complex. In this spectroscopy, one determines the dependence of the shallow ZPH depth on λ_B under constant burn fluence conditions.[18,22] It has been assumed that a possible dependence of S on burning wavelength and quantum yield within a particular state has negligible effect on the action spectrum, given that action spectra are always obtained with very low fluence and burning from the red to blue to minimize a small contribution from broad nonresonant low-energy side-band hole.

The insert of Figure 6 shows constant fluence hole-burned spectra obtained for different burn wavelengths in the low-energy region of the CP43 absorption spectrum of sample 3. These data are used to generate the ZPH-action spectrum shown as diamonds in Figure 6 (which indicate the hole depth at a particular burn wavelength). The thick solid line corresponds to the low-energy region of the CP43 absorption spectrum at

CP43 Antenna Complex of Higher Plant Photosystem

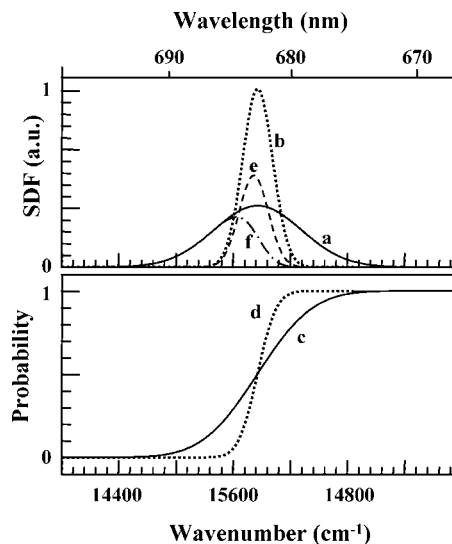*J. Phys. Chem. B, Vol. 112, No. 32, 2008* **9927**
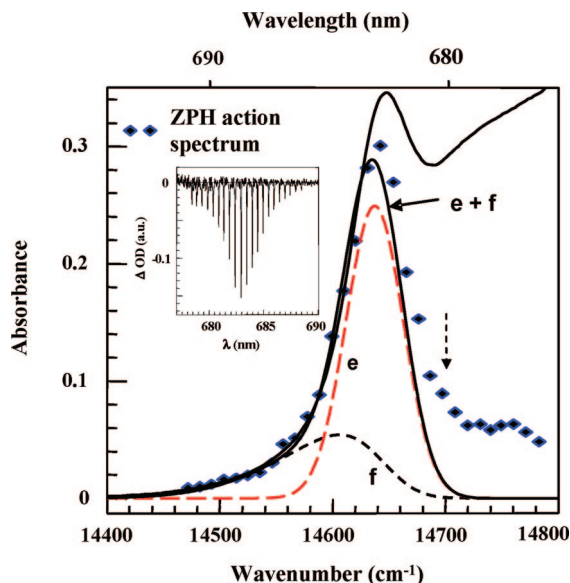
Figure 6. Hole-burning action spectrum (diamonds) for sample 3. Normalized absorption spectrum is presented for comparison. Long-dashed spectrum (curve e) and short-dashed spectrum (curve f) correspond to the contributions of B and A chlorophylls to the action spectrum, respectively. Solid line spectrum labeled as (e + f) represents the fit to the action spectrum. Dashed arrow indicates higher energy contribution to the action spectrum.

Figure 7. Curves a and b represent the "true" SDF of the two lowest-energy states in CP43. Curve c is the probability that an A-type chromophore has its ZPL at energy lower than the corresponding energy of the x-axis. Curve d is the probability that a B-type chromophore has its ZPL at energy lower than the corresponding energy of the x-axis. Curve e is the SDF of the ensemble of the B-type chromophores, which are the lowest-energy chromophores in their complexes. Curve f is the SDF of the ensemble of A-type chromophores that are the lowest-energy chromophores in their complexes.

4.2 K. The widths of the ZPHs of the ZPH-action spectrum were limited by a read resolution of 0.5 cm^{-1}. The height of the ZPH-action spectrum was normalized to fit the absorption spectrum in the long-wavelength region ($\lambda > 683$ nm). (Curves e and f will be discussed in the next section.) From these data, one observes that the action spectrum has a maximum near 683 nm, as illustrated by diamonds (corresponding to hole depths) in Figure 6. We note that the tailing of the ZPH-action spectrum is in good agreement with the low-energy absorption spectrum and consistent with our earlier data. On the other hand, our earlier data revealed a slightly broader ZPH action spectrum, thus again indicating a relatively smaller contribution from the B$_s$ sub-bands in our "old" CP43 preparations.[18] The amount of tailing of this spectrum at high burn frequencies (dashed arrow) was stronger in partly contaminated or denatured preparations (data not shown). The ZPH action spectrum obtained for sample 2 (data not shown) was slightly broader with more contribution near 685 nm, suggesting that HB is also possible for aggregates of CP43 complexes, although with much smaller quantum yield than that observed for monomeric complexes.

4. Discussion

4.1. Model for Excitation Energy Transfe between Two Quasi-Degenerate, Lowest-Energy States. As mentioned in the Introduction, excitonic simulations based on the recent high-resolution structure of PSII, as well as CD data from ref 24 argue against the existence of a broad low-energy excitonic band with an oscillator strength equal to that of 3−4 Chl molecules, first proposed in ref 25 and utilized in our earlier analysis of the model for EET in CP43.[22] As an alternative, in this manuscript, we explore the compatibility of our new results with the BMA1 model of ref 24, with the lowest excitonic state of the B-multimer (BM) having an oscillator strength of about one Chl equivalent by coincidence, or with a B1A1 model.[18]

To describe theoretically the optical spectra (vide supra) discussed in this manuscript, we use the excitation energy transfer model as originally described in ref 22. That is, we

take into account EET between quasidegenerate A and B states of CP43 that have uncorrelated SDFs. In this model, we assume that emission, zero-phonon action, and transient HB spectra can be represented as a sum of the respective spectra of subensembles of the protein complexes where either pigment [A (curve a) or B (curve b)] may be the lowest-energy one (and therefore incapable of further downhill EET). (Note that the corresponding sub-bands are labeled as A$_s$ and B$_s$ and are observed in various types of experiments described in this manuscript). That is, in the case of the CP43 complex, A$_s$ and B$_s$ sub-bands (represented in Figure 7 by curves f and e, respectively) are the lowest-energy bands of these subensembles. With this restriction, the model should account for EET between the two lowest-energy (quasidegenerate) bands in the CP43 complex. For more details, see ref 22.

Briefly, in Figure 7, we consider the EET within a hypothetical system that contains just two chromophores. For simplicity we assume that the interaction between these two chromophores is sufficiently weak to prevent delocalization of the excited states but sufficiently strong to allow for EET on a time scale of ~10 ps (i.e., 2 orders of magnitude faster than the typical fluorescence lifetime of chlorophylls in photosynthetic complexes). To model the CP43 complex, we assumed that the site excitation energies for the two chromophores (contributing to bands A and B), labeled as curves a and b in Figure 7, have different SDFs (with different widths) that are completely uncorrelated, in accordance with experimental data.[18] Thus, curves a and b in Figure 7 describe two different chromophores that represent the "true" SDFs of the A and B pigments of CP43. In a given complex, either chromophore could be lower in energy, and their energies are independent. Curve c (or d) is the probability that a chromophore A (or B) has its ZPL at some energy lower than the corresponding energy of the x-axis. For high-energy values, the probability that the chromophore will be lower in energy approaches 1; at low energies, the probability that the chromophore will be lower in energy approaches zero. The probability (as a function of frequency) that a given B-type pigment

**TABLE 1: Parameters of the SDF of Various Bands and Sub-bands**

band	A (curve a)	B (curve b)	A_s (curve f)	B_s (curve e)	curve (e + f)[a]
peak (cm^{-1}/nm)	14 643/ 682.9	14 644/ 682.9	14 607/ 684.6	14 637/ 683.2	14 632/ 683.4
width (cm^{-1})	180	62	107[b]	60	72[b]

[a] With intensity ratio observed for triplet bottleneck hole-burned spectrum, see Figure 8. Somewhat different intensity ratio results in slightly different parameters. [b] fwhm for asymmetric non-Gaussian band.

will be capable of downhill excitation energy transfer is equal to the probability of finding a B-type pigment at a given frequency (curve b) multiplied by the probability of finding an A-type pigment at some lower frequency (curve c); the probability that a given B-type pigment will be incapable of energy transfer is simply 1 minus this probability and is shown as curve e in Figure 7. Similarly, the probability that a given A-type pigment will be incapable of energy transfer is equal to 1 minus the product of curves a and d, and is shown as curve f in Figure 7. In short, curve e is the subensemble B_s of B, which includes only those B-type pigments which are the lowest-energy pigment in their complex. Curve f is the subensemble A_s of A, which includes only those A-type pigments which are the lowest-energy pigment in their complex. We will demonstrate below that consideration of this effect will allow simultaneous fitting of absorption, emission, zero-phonon action, and transient HB spectra, thus providing more insight into the electronic structure and dynamics of CP43 complexes.

4.2. ZPH-Action Spectra. Since ZPH-action spectra yield information directly about the site distribution functions of various pigments, as long as the electron−phonon coupling is weak, their analysis does not require detailed knowledge of electron−phonon coupling and will be performed first. In Figure 6, the long-dashed and short-dashed curves, e and f, respectively, are the fractions of bands B and A, which include only the lowest-energy chromophores, that is, the B_s and A_s sub-bands, respectively. The relative intensities of curves e and f have been adjusted to achieve better fit. This is justified, since various data (see Figures 3 and 4) indicate that the HB yield of sub-band B_s is somewhat larger than that of the sub-band A_s. Thus, a very good fit of the ZPH-action spectrum with curves e and f clearly indicates that the ability to burn holes of dephasing-limited width (∼2 GHz at 4.2 K) into the substates (A_s and B_s) within the A and B absorption region does not prove that EET between A and B is slow, but is merely the consequence of the SDF of bands A and B being uncorrelated. Every CP43 complex contains both A and B chromophores, which are connected by fast EET but contribute to either the A_s or B_s sub-band, not both. As a result, the holes burnt in this region correspond almost entirely to pigments that are incapable of energy transfer so that the hole width is dephasing-limited. EET between B_s and A_s sub-bands is impossible within our model, which is in perfect agreement with our experimental data. The parameters of the two original A and B SDF are presented in Table 1.

4.3. Calculated Absorption and Transient HB Spectrum. As mentioned in the previous section, the shape of the triplet bottleneck holes is not affected by photoproduct absorption, and therefore, these spectra are more easily fitted than saturated persistent holes. We will demonstrate that the same set of parameters for A and B site distribution functions, first employed to fit HB action spectra, can also be employed to simultaneously fit the triplet bottleneck hole spectrum and the low-energy part of the absorption spectrum of CP43. Unlike in ref 22, our model now also includes the effects of electron−phonon coupling. In general, both delocalized protein phonons and localized chlorophyll vibration modes affect the shape of the absorption spectrum. From the viewpoint of the current discussion, coupling
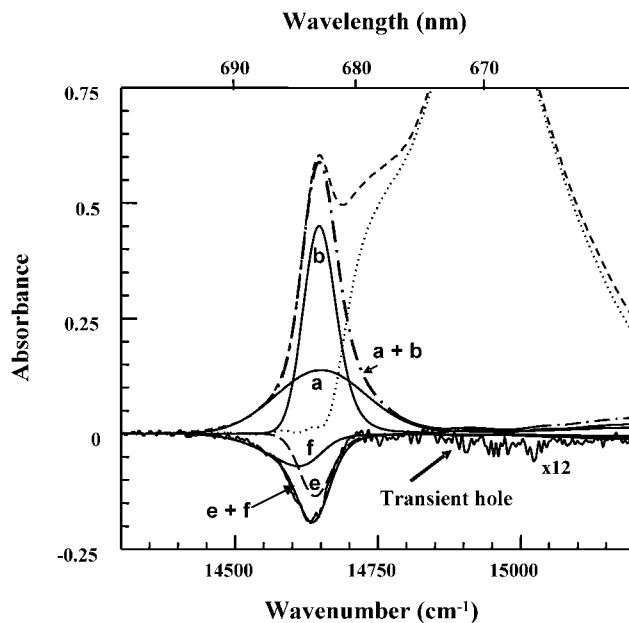
Figure 8. Absorption (dashed curve) and triplet bottleneck hole (noisy solid curve) spectra of sample 3. Curves a and b are absorption spectra (i.e., dressed with phonons and vibrations) of states A and B, respectively. The dash-dotted curve (a + b) is the sum of curves a and b, with relative intensities slightly adjusted for better fit. The dotted curve is the difference between the absorption spectrum and the a + b curve. Curves f and e are contributions to the triplet bottleneck hole, also dressed with phonons, of A and B chromophores, respectively. The relative intensities of these two bands have been normalized to allow for best fit to the triplet bottleneck hole. See text for details.

to the delocalized phonons is the most important element for the shifting of absorption (or hole) spectra bands relative to their respective SDF. Localized chlorophyll modes have to be taken into account to correctly determine the intensities (in Chl equivalents) of various bands. They also play a role in EET, as they affect spectral overlap integrals in the Förster energy transfer equation. We used the frequencies and Huang−Rhys factors of the local modes of Chl *a* as determined for plant PSI particles by Gillie et al.[32–34] using SHB. As demonstrated by Zucchelli et al.,[35] the S factors obtained via SHB allow for a much better fit for the absorption spectra of Chl *a* in various solvents than factors determined via fluorescence line-narrowing (FLN) spectroscopy.

Concerning low-frequency phonon sidebands, it has been reported by Hughes et al.[36] that the phonon sidebands associated with bands A and B peak at 15 and 24 cm^{-1}, respectively, and that for both bands, the Huang−Rhys factor is ∼0.25 (weak electron−phonon coupling). More details about the shape of the phonon sidebands of A and B bands could be determined by fitting the hole spectra resulting from resonant laser irradiation. However, this is not an easy task. At ∼683 nm, both A and B bands are accessed simultaneously; the broad feature to the red from the burn wavelength is contributed to by both the pseudophonon sideband (PSB) of the resonantly burned B_s sub-bands and by A_s sub-bands burned via energy transfer from B. Additionally, photoproduct is obviously present both to the blue

CP43 Antenna Complex of Higher Plant Photosystem

*J. Phys. Chem. B, Vol. 112, No. 32, 2008* **9929**

TABLE 2: Parameters of single-site spectra for pigments contributing to the A- and B-type bands. Vibronic modes were obtained from Refs 32—34

band	ZPL width (cm^{-1})	Huang—Rhys factor (S)	PSB peak frequency (cm^{-1})	Gaussian PSB width[a] (cm^{-1})	Lorentzian PSB width[a] (cm^{-1})
A	0.05	0.30	16	10	30
B	0.05	0.25	24	15	25

[a] The phonon sideband is assumed to be Gaussian on the low-energy side and Lorentzian on the high-energy side of the PSB peak.

and to the red of the resonant hole, affecting the pseudo-PSB shape. The latter problem persists at all wavelengths, including those longer than 686 nm where contribution of the B band to the spectra is negligible.[24] Note that within the framework of our model for EET between two quasidegenerate states, the small contribution of the B band, which might still be present at 686 nm, belongs almost completely to B_s-type pigments, being the lowest-energy pigments in the complex and therefore incapable of downhill energy transfer. Consequently, contrary to the suggestion of ref 24, downhill energy transfer followed by photoconversion does not contribute to the low-energy sideband in the respective HB spectrum, and the whole lower-energy sideband is, in fact, the PSB hole. The absence of EET processes at these long wavelengths is, in fact, supported by the data in ref 24, indicating that the gap between the burn wavelength and the wavelength where the pseudo-PSB feature peaks tapers off and stays constant at burn wavelengths longer than 684 nm. Thus, fitting of the spectral holes according to the theory by Hayes et al.[37] will give the phonon sideband parameters unaffected by EET, at least for λ_B = 686 nm (A band). The parameters for the B band are subject to more error because they result from disentangling A and B contributions for λ_B = 683 nm. The parameters of the phonon sidebands for A and B bands are presented in Table 2.

Taking the above into account, one can dress the SDF of the original A and B bands (for the absorption spectrum; curves a and b in Figure 8, respectively) and of sub-bands A_s and B_s (triplet bottleneck hole spectra; curves f and e in Figure 8) with phonons and vibrations and fit the respective spectra. An additional challenge to perfectly fit data presented in Figure 8 included the requirement that the integral intensities of both low-energy bands should be close to one chlorophyll equivalent. As stated in Section 4.1, we are exploring the compatibility of our results with the BMA1 model of ref 24 with lowest excitonic state of the B-multimer having oscillator strength of about one Chl equivalent, or alternatively, with a B1A1 model (see also our discussion on the results of ref 24, below). Additionally, we required that the difference between the CP43 absorption spectrum and the sum of the absorption spectra of the two lowest-energy states should not exhibit any unphysical kinks (see the dotted curve for the remaining absorption of CP43). The dotted curve exhibits an obvious shoulder due to the band peaked at ~678 nm, matching the weak shoulder in the absorption spectrum. The parameters of the SDF of the two lowest-energy bands are the same as presented in Table 1. Thus, here, we demonstrate that our spectroscopy results are also fully consistent with the BMA1 model. Unfortunately, this means that one cannot draw a definite conclusion on whether the B1AM or BMA1 or B1A1 model is more correct on the basis of data presented in this manuscript. This issue, however, will be revisited in the accompanying paper, where detailed excitonic calculations are presented and discussed. Note that in ref 24, within the frame of the BMA1 model, the lowest state of the B near 683 nm is contributed to by several Chls and has the oscillator strength of about one chlorophyll equivalent just by a coincidence. Curves a and b in Figure 8 correspond to the
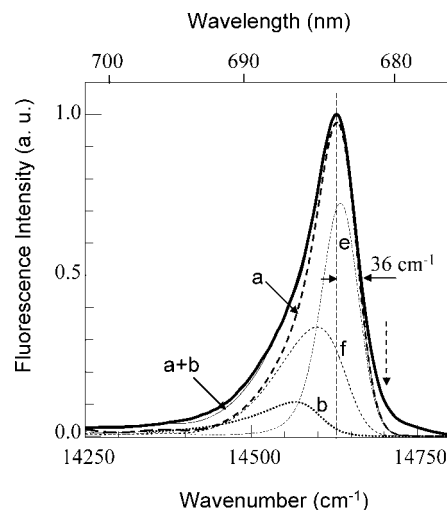
Figure 9. Emission spectrum of sample 3 (solid curve). Curve a is the sum of curves e and f from Figure 7, dressed with phonons. Curve b represents the emission spectrum of deliberately aggregated CP43 sample. The sum of curves a and b, with properly adjusted intensities, yields a good fit to the observed emission spectrum of the higher-quality CP43 sample.

true absorption spectra of the two lowest-energy states of CP43, A and B. Curve a + b fits very well the low-energy part of the absorption spectrum. As in Figure 7, curve e is the absorption spectrum of a subensemble of B-type pigments (i.e., sub-band B_s), which are the lowest-energy pigments in their complexes, and curve f represents the absorption spectrum of a subensemble of A-type pigments (i.e., sub-band A_s), which are the lowest-energy pigments in their complexes. As in the case of the HB action spectrum, the intersystem crossing yields might be different for different chromophores, which justifies slight adjustments of the relative intensities of curves e and f in Figure 8. Thus, as expected, the sum of spectra e and f fits very well the transient HB spectrum (solid line; noisy curve) obtained with burning wavelength of 496.5 nm.

4.4. Comparison of Calculated Emission Spectra with Experiment. The 4.2 K fluorescence spectra of CP43 obtained with a burning wavelength of 496.5 nm are shown in Figure 9 (thick solid line). Spectrum a is the sum of curves e and f from Figure 7 but dressed with phonons and localized vibrations and represents the theoretically predicted fluorescence spectrum based on the model of uncorrelated EET between states A and B. The relative intensities of curves e and f have been slightly adjusted for better fit. A discrepancy is clearly observed on the lower-energy side when compared with the measured emission spectrum. Spectrum a, however, does not account for the emission from the aggregated CP43 complexes. We have already suggested above that a small contribution from aggregated CP43 complexes could not be excluded (see Figure 2, frame B). This is confirmed by curve b of Figure 9 (thick dotted line), which corresponds to the measured emission spectrum of deliberately aggregated CP43 sample. Similar fluorescence spectra were already reported by taking a difference between the fluorescence

spectra of CP43 samples with different degrees of aggregation (i.e., with different concentrations of detergent).[18] A somewhat larger contribution from aggregates to the emission spectrum shown in Figure 9, as compared with absorption and persistent hole-burned spectra, suggests that fluorescence quantum yield increases upon aggregation, in agreement with fluorescence excitation spectra (data not shown). As expected, the sum of curves a and b (labeled as the a + b spectrum) describes the experimentally measured fluorescence spectrum (solid line) very well. Note that the half-width of the fluorescence spectrum estimated on the high-energy side is only 36 cm^{-1}. When the contribution at 676 nm has been eliminated from the previously measured fluorescence spectrum,[18] nearly an identical half-width of the high-energy side has been obtained. As previously mentioned, spectrum a contains the contribution from both A_s and B_s sub-bands and is consistent with our EET model discussed above. The frequency difference (of ~13 cm^{-1}) between the maxima of absorbance and fluorescence spectra is a result of interplay between two effects. First, it is obviously an indication of weak coupling to the low-energy phonons for a narrow B band, S ~ 0.25.[18] Second, we recall that the absorption spectrum is contributed to by the "true" bands A and B, whereas the emission originates from subensembles A_s and B_s. Finally, we comment on the minor differences between the fluorescence spectra shown in Figure 2B and C; that is, curves 3 and b, respectively. The fwhm of spectrum b, obtained in CE buffer at 4.2 K, is broader by a factor of ~1.2 than the fluorescence spectrum obtained off-line in a glycerol/buffer glass; the latter is due to a solvent effect (i.e., different matrix composition). However, its more symmetric shape suggests that the online measured fluorescence spectrum does not contain a contribution from aggregated CP43 complexes. The higher-energy discrepancy between the calculated and experimental spectra (see dashed arrow) may be attributed to a very minor contaminant (compare with spectra 1 and 2 in Figure 2B) or, at least to some extent, to a small subpopulation of CP43 complexes in which some emission originates from higher-energy excitonic states. That is, for a small number of specific realizations of the energy disorder, emission near 678−679 nm could be observed if the EET from the higher-energy excitonic states to the lowest-energy state is inefficient. These pigments were not included in our simple model treating EET between two pigments with uncorrelated site distribution functions.

4.5. Assignment of the A and B States to Particular Chlorophylls in the Complex. Several chlorophylls have been suggested as possible candidates that mostly contribute to the lowest-energy states in CP43.[23,24] Recent femtosecond visible/visible and visible/midinfrared pump probe spectroscopy experiments suggested that at least some of the red absorbing pigments are located in a polar environment, possibly forming H-bonds with the surrounding protein.[23] Earlier findings also suggested that the narrow-band B is due to a pigment that is in H-bond contact with its environment,[24] primarily on the basis of analysis of FLN data and the assumption that a strong hydrogen bond is required to explain a large nonexcitonic shift of the B band. According to Di Donato et al.,[23] the most likely candidates for the lowest-energy chlorophylls include Chl34 (with a possible H interactions with a tyrosine and a histidine), Chl47 (with a 9-keto carbonyl at H-bond distance from an aspartic residue and very close to an arginine residue), and Chl49 (close to a tyrosine residue) in the notation of Loll et al.[8] However, at the current structural resolution (3 Å), the assignment of specific H-bonds is somewhat speculative, particularly since neither hydrogen atoms nor water molecules are resolved. Furthermore,

one should consider the possibility that just the polar environment by itself (for example, for Chl37 and Chl44) or Chl ring deformation[38] could lead to a significant red shift of the Chl origin bands. In addition, ensembles of strongly coupled Chls (such as Chl44, Chl45, and Chl46) could yield lowest-energy states that can also be red-shifted, as originally suggested for the A state in ref 25. Note that the above list unfortunately contains 8 out of 13 Chls constituting the CP43 complex, and thus, additional criteria have to be employed to decrease the number of possible candidates for the low-energy state(s).

The assignment of a very strong hydrogen bond to the 13^1 carbonyl group of the Chl corresponding to the B band led to the suggestion of a possible photoconversion process involving disruption of Chl-protein hydrogen bonding. This photoconversion process is used to explain the appearance of a strong absorption increase near 670 nm in the persistent hole-burning spectra; this suggestion, however, is challenged in this work as well as in the accompanying paper.

Additional information on the possible composition of the A and B states can be obtained from the Stark hole-burning data presented in ref 18. It was shown that band B is characterized by an unusually low response to the electric field ($f\Delta\mu < 0.25$ or even $f\Delta\mu \sim 0$),[18] which may indicate that the respective pigment is in excitonic interaction predominantly with other pigments having anti-parallel transition dipole moments. With this in mind, we find that the most antiparallel transition dipoles are found for the Chl34/Chl37 and Chl34/Chl46 pairs of chlorophylls that are strongly coupled. These pairs are characterized by $\boldsymbol{\mu}_1 \cdot \boldsymbol{\mu}_2 = -0.85$ and -0.99, respectively. Note that on the basis of the X-ray structure, Chl34 is also likely to form a hydrogen bond with tyrosine and histidine residues.[8] However, the above two pairs of chlorophylls exhibit strong interaction energies of 75 and 66 cm^{-1}, respectively. This, combined with an antiparallel dipole orientation, would result in the lowest state of the dimer (or multimer, since both pairs contain Chl34) borrowing oscillator strength from the higher-energy state(s); this effect is more pronounced if transition energies of individual molecules are closer to each other in the absence of excitonic interaction. Such borrowing, however, is inconsistent with the experimental results indicating that the oscillator strength of the B-band is approximately equivalent to that of one chlorophyll molecule. However, if the site energies of the two pigments are energetically separated, the borrowing of oscillator strength should be relatively small. As a result, any one of these chlorophylls (i.e., 37, 34, and 46) could contribute strongly to the B band, although the remaining two pigments should probably be blue-shifted (see the accompanying paper). It is also important to mention that such strong pairwise couplings would be incompatible with the assignment of Hughes et al.,[24] who placed the three excitonic components of the B-multimer at 683, 680, and 676 nm. Therefore, before we move forward with our discussion, it seems appropriate to comment on the data by Hughes et al.[24] in a more detailed fashion. The key issue discussed there was the analysis of the shape of the difference in the CD spectra resulting from illumination with 488 nm light; these low-temperature (1.7 K) ΔCD spectra could be successfully fitted with three components associated with the chlorophyll multimer, the lowest-energy state being the B state.[24] A fourth component, corresponding to the monomeric A-state at 683 nm, was required to simultaneously fit the absorption spectrum. This led to the idea of BMA1 model. Unfortunately, we find the above approach quite problematic. First, in the view of the results presented above, it appears to us that Hughes et al.[24] did not account for NPHB photoproduct

TABLE 3: Coupling Constants (V_{nm}; in cm^{-1})[a] between Chlorophylls in the PSII Reaction Center and CP43 Complex

pigment	Chl33	Chl34	Chl35	Chl37	Chl41	Chl42	Chl43	Chl44	Chl45	Chl46	Chl47	Chl48	Chl49
P_1	−0.9	1.9	1.3	−4.1	−3.0	−0.8	−1.4	−1.9	1.0	−2.6	−1.4	0.2	−0.7
P_2	0.9	−0.4	−0.8	2.3	3.5	0.7	1.3	−1.9	−0.3	1.0	0.1	−0.7	0.6
Chl_1	1.7	−2.0	−0.3	1.8	7.0	0.5	2.3	−0.6	−1.4	1.9	0.3	−0.4	0.7
Chl_2	−0.4	−0.3	1.3	−2.3	−2.2	−0.7	−0.9	0.3	0.2	−1.1	−1.2	0.5	−0.6
$Pheo_1$	−0.5	−0.4	0.2	−0.3	−6.7	−0.8	−1.3	6.3	0.5	−0.3	1.0	1.0	−0.5
$Pheo_2$	−0.2	0.8	−0.8	0.0	0.5	0.4	0.1	0.4	0.4	−0.4	1.0	−0.3	0.2
Chl_{z1} [b]	2.1	−1.0	−0.3	0.9	7.7	0.2	4.7	−0.3	−2.0	1.4	0.0	−0.7	0.8

[a] Calculated using a dipole strength of 18.5 D^2 (Chl *a*) and 11.1 D^2 (Pheo *a*). [b] Chl_{z2} on the opposite side of the complex (i.e., D2) is not included, since interactions involving this Chl are even weaker than those for $Pheo_2$.

contributions in the ΔCD spectra. That is, a significant amount of the NPHB photoproduct is distributed in the immediate vicinity of the original hole, as shown in Figures 3, 4, and 6. It is reasonable to expect that the magnitude of the CD is the same for photoproduct as for educt in the case of NPHB, and therefore, some contributions to ΔCD spectra should be ascribed to photoproduct. Second, the measurement of the differences in CD spectra resulting from nonresonant illumination is similar to regular hole-burning measurements in that the pigments with the highest hole-burning (or photoconversion) yield are probed preferentially as they burn first.[18,24] In other words, the underlying physical principle responsible for observed changes in the above-discussed ΔCD spectra is the same in both cases (i.e., NPHB and ΔCD experiments). Only the means to detect these changes differ. Therefore, we believe that the CD experiments described by Hughes et al.[24] are subject to the same kind of misinterpretation as was made in our own earlier work involving conventional HB experiments,[18] in which the subensembles (sub-bands) A$_s$ and B$_s$ were mistaken for the true bands A and B. Although we do not reject the hypothesis that the B state has some excitonic character (see the accompanying paper), which is supported by the CD results,[24] the parameters of the higher-energy excitonic components of state B (our notation) as presented in ref 24 are, in our opinion, subject to large errors. For example, the 680 nm hole observed in ref 24 most likely does not belong to excitonically coupled pigments of the monomeric CP43 complexes because its relative intensity with respect to the 683 nm hole appears to be highly sample-dependent in our HB experiments, and as mentioned above, it is hardly visible in spectra shown in Figures 3 and 4.

On the other hand, antiparallel orientation of the dipole moments is not the only possible explanation for the unusual properties of the B-band. Namely, it can be deduced from the Stark hole-burning experiments that $f\Delta\mu$ of the pigments in photosynthetic complexes has significant matrix-induced contribution.[18] That is, almost without exception, spectral holes in photosynthetic complexes broaden but do not split in the electric field.[39] (Very strong matrix-induced contribution to $f\Delta\mu$ leads to strong hole-broadening). The unusually low response of the B band to an electric field could also be a result of a relatively weak matrix-induced contribution to $f\Delta\mu$. This interpretation would be in agreement with the small inhomogeneous width of band B (see Table 1) caused by a smaller degree of disorder. However, excitonic calculations and modeling of various types of experimental spectra are needed to narrow the pool of Chl contributing to the B band, as discussed in the accompanying paper.

Our previous studies of the CP43′−PSI supercomplexes[26] indicated that B pigment(s) (i.e., Chl(s) contributing to band B) are more likely to transfer energy to A pigment(s) (i.e., Chl(s) contributing to band A) than to the PSI core, and this transfer occurs on a time scale on the order of 10 ps. To achieve the

latter result, the coupling matrix element between chlorophylls contributing to bands A and B should be ∼10 cm^{-1}. It is also preferable for the pigment contributing to band A to be situated closer to the PSI core in the PSI−CP43′ supercomplex than the pigment contributing to the B band. We note that the cryomicroscopy results indicate that the CP43′ units are oriented in relation to the PSI core in the same way the CP43 units are oriented in relation to the reaction center in PSII.[40]

The chlorophylls closest to the PSII RC (or PSI core) are Chl 41 and Chl 44. The couplings between the chlorophylls of CP43 and those of the PSII RC are presented in Table 3 (Chl_{z2} on the other side of the RC is ignored). These coupling constants are calculated in the dipole−dipole approximation, since the distances between the pigments are >20 Å. One can see that although Chl 41 exhibits the strongest coupling to the RC Chl pigments, Chl 44 is also strongly coupled to Pheo D1. As a result, although Chls 37, 43, and 46 (proposed band B Chls) also show weak coupling to various RC pigments, it appears that Chls 41 and Chl 44 are better candidates for the A state. Note that the highest couplings in the Table 3 are ∼8 cm^{-1}, in agreement with the relatively low (on the order of tens of picoseconds) CP43 → RC EET rates observed for intact oxygen-evolving PSII core complexes at low temperature.[41]

Finally, we note that the triplet bottleneck HB spectrum shown in Figure 5 contains, in addition to the asymmetric low-energy hole, a broad and structureless band near 670 nm (arrow). Such a broad bleach with a maximum near 670 nm is, in fact, of great importance, since it should also allow us to narrow the choice of possible candidates for states A and B. This, however, is beyond the scope of this manuscript and is discussed in the accompanying paper. Here, we only mention that the fact that both the main hole peaked at 683 nm and its weak companion hole near 670 nm have the same sign indicates that the oscillator strength associated with the Chl molecule(s) on which the triplet is localized is distributed between short and long wavelengths. (From Figure 8, it is obvious that the higher-energy vibronic replicas of the main triplet-bottleneck hole are too weak to account for the 670-nm feature; the match between the experimental and calculated triplet bottleneck holes is perfect at <660 nm. This is also an additional proof that higher excitonic components of the lowest-energy states lie near 670 nm, and not at 676−680 nm.) In other words, higher-energy chlorophylls in intact CP43 are stealing some oscillator strength from the lowest-energy ones. (In the opposite situation, removal of the lowest-energy chlorophyll from the ensemble (by triplet bottleneck HB) would result in migration of formerly stolen oscillator strength to higher energies, and a positive feature, rather than bleach, would appear near 670 nm, as observed for several Chl combinations in excitonic calculations (see the accompanying paper). This also provides a feasible explanation for the increased absorption at 670 nm in persistent hole-burned spectra: as lowest-state pigments are shifted slightly to the blue (via

regular nonphotochemical hole burning), the interaction between the low-energy Chl and its higher-energy excitonic partners is increased (due to closer site energies), resulting in the "stealing" of more intensity by the higher-energy states. This possibility is discussed in more detail in the accompanying paper. Another consequence of this stealing of oscillator strength by higher-energy Chls is that one would expect the lowest energy state of CP43 (which may be localized on different Chls in different individual complexes; represented by the sum of curves e and f in Figure 8) to have average oscillator strength somewhat lower than the equivalent of one chlorophyll. Comparing the integrated area of the transient hole shown in Figure 5 (curve a) and obtained from our best CP43 sample, one may estimate the oscillator strength of the lowest-energy band as 0.7 ± 0.2. The error margin is quite high, since two different chlorophylls contributing to the lower-energy triplet bottleneck hole may have different intersystem crossing rates (see the accompanying paper for more details).

4.6. Implications for EET in the CP43′−PSI Supercomplex. Structural data on the CP43′−PSI supercomplex[40] suggests that the distances between the identical chlorophylls of adjacent CP43′ monomers are ~40 Å; that is, only slightly larger than the distances between CP43′ chlorophylls closest to the PSI core and the core chlorophylls. Due to the 18-fold symmetry of the CP43′ ring, the angles between the transition dipole moment vectors of structurally identical chlorophylls are only 360/18 = 20 degrees. As a result, the orientation factors, which affect the interaction energies, should be large. The spectral overlap between absorption and emission spectra of identical chlorophylls is also most likely quite large, especially for pigment B, whereas the spectral overlap with core pigments close to CP43′ is expected to be small. In fact, we have already assigned a minor derivative-like feature in the supercomplex-minus-core spectrum at 695 nm to some core chlorophyll shifted as a result of interaction with CP43′.[26] In light of the above, it becomes possible that A → A′ and especially B → B′ EET rates within the CP43′ manifold are larger than the CP43′ → PSI core EET rate, even at low temperature. Thus, every A or B chlorophyll of a given CP43′ monomer may have several options for transfer. In addition to transferring energy to the core and to its own B/A partner (if the latter is lower in energy), each A or B pigment can (although with somewhat smaller probability) transfer energy also to A or B of the adjacent CP43′ unit. Of course, inter-CP43′ excitation hopping would be further facilitated if A → B′ and B → A′ EET between adjacent CP43′ units is also possible. Qualitatively, these processes will result in excitation traveling through several units in the CP43′ ring before it reaches one of the local lowest energy state(s) of the CP43′ manifold. (Note that there are 18 CP43′ units per supercomplex and that PSI core is trimeric. Thus, there are six nonequivalent positions of the CP43′ unit with respect to the PSI core.) The emission (and low-fluence action) spectra in ref 26 are then due to those pigments which simultaneously are (a) the lowest-energy pigments, not only in their own CP43′, but also among its closest neighbors; and (b) in an unfortunate position in relation to the core. This would explain the shift of emission beyond 685 nm,[26] despite the higher-fluence action spectrum's being peaked at 682 nm and electron−phonon coupling's being weak.

5. Conclusions

Absorption, emission, zero-phonon action, and transient HB spectra can be well-fitted by allowing for energy transfer between the two lowest energy bands A and B in CP43. In this model (B1A1), fluorescence, zero-phonon action, and transient HB spectra can be represented by a sum of the subensembles of the CP43 complexes, in which either of the two low-energy bands may be the lowest-energy state incapable of downhill energy transfer. Our results are consistent with ~10 ps EET from state B to state A in CP43. EET in a particular complex is possible either from A to B or from B to A. The shape of the transient spectrum is an inverted image of the absorption spectrum of a subensemble of B_s-type and A_s-type pigments, respectively, which are the lowest-energy pigments in their complexes. We have demonstrated that the major emission band originates from sub-bands A_s and B_s, whereas the absorption spectrum is contributed to by the "true" A and B bands. We have also proposed that the high-energy photoproduct in persistent HB spectra originate from regular NPHB accompanied by the redistribution of oscillator strength due to modified postburn excitonic interactions. We have argued that the photoconversion process (suggested to occur via tunneling between alternate configurations of the C=O−H−protein hydrogen bond when the molecule is in the excited state,[24]), while feasible, is not required to account for the strong positive absorption increase in the saturated HB spectra (further evidence is provided in the accompanying paper). Finally, on the basis of the above discussion, it appears that the best candidates from the 13 Chls of the CP43 complex that mostly contribute to the B band are Chls 34, 37, and 46, and that Chls 41 and 44 are likely to contribute to the A band. However, definite assignments cannot be made on the basis of this data alone. The choice of Chls contributing to the low energy states can be further narrowed by simultaneous fitting of the absorption and emission spectra and transient/persistent HB spectra using excitonic calculation as demonstrated and discussed in detail in the accompanying paper.

Abbreviations

Chlorophyll, Chl; energy, E; capillary electrophoresis, CE; excitation energy transfer, EET; fluorescence line-narrowing, FLN; full width at half-maximum, fwhm; hole burning, HB; Huang−Rhys factor, S; inhomogeneous broadening, Γ_{inh}; laser-induced fluorescence, LIF; nonphotochemical hole burning, NPHB; photosynthetic complexes, PC; photochemical hole burning, PHB; phonon sideband, PSB; photosystem I, PSI; photosystem II, PSII; reaction center, RC; site distribution functions, SDF; spectral hole-burning, SHB; temperature, T; zero-phonon hole, ZPH; zero-phonon line, ZPL.

References and Notes

(1) Schelvis, J. P. M.; van Noort, P. I.; Aartsma, T. J.; van Gorkom, H. J. Energy Transfer, Charge Separation and Pigment Arrangement in the Reaction Center of Photosystem II. *Biochim. Biophys. Acta* **1994**, *1184*, 242–250.

(2) Blankenship, R. E. In *Molecular mechanisms of photosynthesis*; Blackwell Science: Oxford, Malden, MA, 2002; Chapters 4−6; pp 42−123

(3) Barber, J.; Morris, E.; Büchel, C. Revealing the Structure of the Photosystem II Chlorophyll Binding Proteins, CP43 and CP47. *Biochim. Biophys. Acta* **2000**, *1459*, 239–247.

(4) Vasil'ev, S.; Orth, P.; Zouni, A.; Owens, T. G.; Bruce, D. Excited-State Dynamics in Photosystem II: Insights from the x-Ray Crystal Structure. *Proc. Natl. Acad. Sci. U.S.A.* **2001**, *98*, 8602–8607.

CP43 Antenna Complex of Higher Plant Photosystem

J. Phys. Chem. B, Vol. 112, No. 32, 2008 **9933**

(5) Bricker, T. M.; Frankel, L. K. The Structure and Function of CP47 and CP43 in Photosystem II. *Photosynth. Res.* **2002**, *72*, 131–146.

(6) Eijckelhoff, C.; Dekker, J. P.; Boekema, E. J. Characterization by Electron Microscopy of Dimeric Photosystem II Core Complexes from Spinach with and without CP43. *Biochim. Biophys. Acta* **1997**, *1321*, 10–20.

(7) Zouni, A.; Witt, H. T.; Kern, J.; Fromme, P.; Krauss, N.; Saenger, W.; Orth, P. Crystal Structure of Photosystem II from *Synechococcus elongatus* at 3.8 Å Resolution. *Nature* **2001**, *409*, 739–743.

(8) Loll, B.; Kern, J.; Saenger, W.; Zouni, A.; Biesiadka, J. Towards Complete Cofactor Arrangement in the 3.0 Å Resolution Structure of Photosystem II. *Nature* **2005**, *438*, 1040–1044.

(9) Ferreira, K. N.; Iverson, T. M.; Maghlaoui, K.; Barber, J.; Iwata, S. Architecture of the Photosynthetic Oxygen-Evolving Center. *Science* **2004**, *303*, 1831–1838.

(10) Bricker, T. The Structure and Function of CPa-1 and CPa-2 in Photosystem II. *Photosynth. Res.* **1990**, *24*, 1–13.

(11) Boekema, E. J.; Van Roon, H.; Van Breemen, J. F. L.; Dekker, J. P. Supramolecular Organization of Photosystem II and its Light-Harvesting Antenna in Partially Solubilized Photosystem II Membranes. *Eur. J. Biochem.* **1999**, *266*, 444–452.

(12) Yamamoto, Y.; Akasaka, T. Degradation of Antenna Chlorophyll-Binding Protein CP43 during Photoinhibition of Photosystem II. *Photosynth. Res.* **1995**, *4*, 267–270.

(13) Neale, P. J.; Melis, A. Dynamics of Photosystem II Heterogeneity during Photoinhibition: Depletion of PS IIβ from Non-Appressed Thylakoids during Strong-Irradiance Exposure of *Chlamydomonas reinhardtii*. *Biochim. Biophys. Acta* **1991**, *1056*, 195–203.

(14) Mori, H.; Yamashita, Y.; Akasaka, T.; Yamamoto, Y. Further Characterization of the Loss of Antenna Chlorophyll-Binding Protein CP43 from Photosystem II during Donor-Side Photoinhibition. *Biochim. Biophys Acta* **1995**, *1228*, 37–42.

(15) Rhee, K.; Morris, E. P.; Zheleva, D.; Hankamer, B.; Kuhlbrandt, W.; Barber, J. Two-Dimensional Structure of Plant Photosystem II at 8 Å Resolution. *Nature (London)* **1997**, *389*, 522–526.

(16) Delepelaire, P.; Chua, N. Lithium Dodecyl Sulfate/Polyacrylamide Gel Electrophoresis of Thylakoid Membranes at 4 DegC: Characterizations of Two Additional Chlorophyll *a*-Protein Complexes. *Proc. Natl. Acad. Sci. U.S.A.* **1979**, *76*, 111–115.

(17) Chua, N.; Bennoun, P. Thylakoid Membrane Polypeptides of *Chlamydomonas reinhardtii*. Wild-Type and Mutant Strains Deficient in Photosystem II Reaction Center. *Proc. Natl. Acad. Sci. U.S.A.* **1975**, *72*, 2175–2179.

(18) Jankowiak, R.; Zazubovich, V.; Ratsep, M.; Matsuzaki, S.; Alfonso, M.; Picorel, R.; Seibert, M.; Small, G. J. The CP43 Core Antenna Complex of Photosystem II Possesses Two Quasi-Degenerate and Weakly Coupled Q_y-Trap States. *J. Phys. Chem. B* **2000**, *104*, 11805–11815.

(19) Alfonso, M.; Montoya, G.; Cases, R.; Rodriguez, R.; Picorel, R. Core Antenna Complexes, CP43 and CP47, of Higher Plant Photosystem II. Spectral Properties, Pigment Stoichiometry, and Amino Acid Composition. *Biochemistry* **1994**, *33*, 10494–10500.

(20) Picorel, R.; Alfonso, M.; Seibert, M. Isolation of CP43 and CP47 Photosystem II Proximal Antenna Complexes from Plants. *Methods Mol. Biol.* **2004**, *274*, 129–135.

(21) Groot, M.; Frese, R. N.; De Weerd, F. L.; Bromek, K.; Pettersson, A.; Peterman, E. J. G.; Van Stokkum, I. H. M.; Van Grondelle, R.; Dekker, J. P. Spectroscopic Properties of the CP43 Core Antenna Protein of Photosystem II. *Biophys. J.* **1999**, *77*, 3328–3340.

(22) Zazubovich, V.; Jankowiak, R. On the Energy Transfer between Quasi-Degenerate States with Uncorrelated Site Distribution Functions: An Application to the CP43 Complex of Photosystem II. *J. Lumin.* **2007**, *127*, 245–250.

(23) Di Donato, M.; van Grondelle, R.; van Stokkum, I. H.; Groot, M. L. Excitation Energy Transfer in the Photosystem II Core Antenna Complex CP43 Studied by Femtosecond visible/visible and visible/mid-Infrared Pump Probe Spectroscopy. *J. Phys. Chem. B* **2007**, *111*, 7345–7352.

(24) Hughes, J. L.; Picorel, R.; Seibert, M.; Krausz, E. Photophysical Behavior and Assignment of the Low-Energy Chlorophyll States in the CP43 Proximal Antenna Protein of Higher Plant Photosystem II. *Biochemistry* **2006**, *45*, 12345–12357.

(25) De Weerd, F. L.; Van Stokkum, I. H. M.; Van Amerongen, H.; Dekker, J. P.; van Grondelle, R. Pathways for Energy Transfer in the Core Light-Harvesting Complexes CP43 and CP47 of Photosystem II. *Biophys. J.* **2002**, *82*, 1586–1597.

(26) Riley, K. J.; Zazubovich, V.; Jankowiak, R. Frequency-Domain Spectroscopic Study of the PS I-CP43′ Supercomplex from the Cyanobacterium Synechocystis PCC 6803 Grown Under Iron Stress Conditions. *J. Phys. Chem. B* **2006**, *110*, 22436–22446.

(27) Jankowiak, R.; Raetsep, M.; Picorel, R.; Seibert, M.; Small, G. J. Excited States of the 5-Chlorophyll Photosystem II Reaction Center. *J. Phys. Chem. B* **1999**, *103*, 9759–9769.

(28) Jankowiak, R.; Roberts, K. P.; Small, G. J. Fluorescence Line-Narrowing Detection in Chromatography and Electrophoresis. *Electrophoresis* **2000**, *21*, 1251–1266.

(29) Roberts, K. P.; Lin, C.; Singhal, M.; Casale, G. P.; Small, G. J.; Jankowiak, R. On-Line Identification of Depurinating DNA Adducts in Human Urine by Capillary Electrophoresis-Fluorescence Line Narrowing Spectroscopy. *Electrophoresis* **2000**, *21*, 799–806.

(30) Miksa, B.; Chinnappan, R.; Dang, N. C.; Reppert, M.; Matter, B.; Tretyakova, N.; Grubor, N. M.; Jankowiak, R. Spectral Differentiation and Immunoaffinity Capillary Electrophoresis Separation of Enantiomeric Benzo(a)Pyrene Diol Epoxide-Derived DNA Adducts. *Chem. Res. Toxicol.* **2007**, *20*, 1192–1199.

(31) Grubor, N. M.; Armstrong, D. W.; Jankowiak, R. Flow-through Partial-Filling Affinity Capillary Electrophoresis using a Crossreactive Antibody for Enantiomeric Separations. *Electrophoresis* **2006**, *27*, 1078–1083.

(32) Gillie, J. K. *Spectral Hole Burning Studies of Photosystem I.* Ph.D. thesis, Iowa State University, 1990, *98*.

(33) Gillie, J. K.; Small, G. J.; Golbeck, J. H. Nonphotochemical Hole Burning of the Native Antenna Complex of Photosystem I (PSI-200). *J. Phys. Chem.* **1989**, *93*, 1620–1627.

(34) Gillie, J. K.; Fearey, B. L.; Hayes, J. M.; Small, G. J.; Golbeck, J. H. Persistent Hole Burning of the Primary Donor State of Photosystem I: Strong Linear Electron-Phonon Coupling. *Chem. Phys. Lett.* **1987**, *134*, 316–322.

(35) Zucchelli, G.; Jennings, R. C.; Garlaschi, F. M.; Cinque, G.; Bassi, R.; Cremones, O. The Calculated in Vitro and in Vivo Chlorophyll *a* Absorption Bandshape. *Biophys. J.* **2002**, *82*, 378–390.

(36) Hughes, J. L.; Prince, B. J.; Arskold, S. P.; Krausz, E.; Pace, R. J.; Picorel, R.; Seibert, M. Photo-Conversion of Chlorophylls in Higher-Plant CP43 Characterized by Persistent Spectral Hole Burning at 1.7 K. *J. Lumin.* **2004**, *108*, 131–136.

(37) Hayes, J. M.; Gillie, J. K.; Tang, D.; Small, G. J. Theory for Spectral Hole Burning of the Primary Electron Donor State of Photosynthetic Reaction Centers. *Biochim. Biophys. Acta* **1988**, *932*, 287–305.

(38) Zucchelli, G.; Brogioli, D.; Casazza, A. P.; Garlaschi, F. M.; Jennings, R. C. Chlorophyll Ring Deformation Modulates Q_y Electronic Energy in Chlorophyll−Protein Complexes and Generates Spectral Forms. *Biophys. J.* **2007**, *93*, 2240–2254.

(39) Hsin, T.; Zazubovich, V.; Hayes, J. M.; Small, G. J. Red Antenna States of PS I of Cyanobacteria: Stark Effect and Interstate Energy Transfer. *J. Phys. Chem. B* **2004**, *108*, 10515–10521.

(40) Melkozernov, A. N.; Barber, J.; Blankenship, R. E. Light Harvesting in Photosystem I Supercomplexes. *Biochemistry* **2006**, *45*, 331–345.

(41) Hughes, J. L.; Prince, B. J.; Krausz, E.; Smith, P. J.; Pace, R. J.; Riesen, H. Highly Efficient Spectral Hole-Burning in Oxygen-Evolving Photosystem II Preparations. *J. Phys. Chem. B* **2004**, *108*, 10428–10439.

(42) Reppert, M.; Zazubovich, V.; Dang, N. C.; Seibert, M.; Jankowiak, R. Low-Energy Chlorophyll States in the CP43 Antenna Pritein Complex: Simulation of Various Optical Spectra. II. *J. Phys. Chem. B* **2008**, *112*, 9934–9947.